Study of the $\Lambda \to p\ell\bar{\nu}_\ell$ Semileptonic Decay in Lattice QCD

Simone Bacchio[1] and Andreas Konstantinou[2]
[1]Computation-based Science and Technology Research Center, The Cyprus Institute, 20 Kavafi Street, Nicosia 2121, Cyprus
[2]Department of Physics, University of Cyprus, P.O. Box 20537, 1678 Nicosia, Cyprus

(Received 15 July 2025; revised 16 October 2025; accepted 10 November 2025; published 2 December 2025)

We present the first lattice QCD determination of the $\Lambda \to N$ vector and axial-vector form factors, which are essential inputs for studying the semileptonic decay $\Lambda \to p\ell\bar{\nu}_\ell$. This channel provides a clean, theoretically controlled avenue for extracting the Cabibbo-Kobayashi-Maskawa matrix element $|V_{us}|$ from the baryon sector. Our analysis uses a gauge ensemble with physical light, strange, and charm quark masses and yields the most precise determination to date of the full set of transition form factors—including second-class contributions—as well as the associated couplings, radii, and the ratio of muon-to-electron decay rates, an observable sensitive to possible nonstandard scalar and tensor interactions. We compare our nonperturbative results with next-to-next-to-leading order expansions in the small parameter $\delta = (m_\Lambda - m_N)/m_\Lambda \approx 0.16$. We find that the common phenomenological approximation of neglecting the q^2 dependence of the form factors leads to a ∼4% deviation in the decay rate. This underscores the critical importance of precise, fully nonperturbative form factor inputs for achieving the subpercent precision targets of upcoming experimental programs.

DOI: 10.1103/bvs9-wcsj

Introduction—The semileptonic decay $\Lambda \to p\ell\bar{\nu}_\ell$ is one of the weak decay modes of the Λ hyperon, where the valence strange quark of the Λ transforms into an up quark via the weak interaction emitting a virtual W boson that subsequently decays into a lepton-neutrino pair. This process provides a valuable probe of the weak interactions and hadron structure. From a theoretical perspective, the total decay amplitude can be factorized into two components: the hadronic matrix element, describing the $\Lambda \to p$ transition and the leptonic matrix element. The resulting decay amplitude is

$$\mathcal{M} = \frac{G_F}{\sqrt{2}} V_{us} \langle p|\bar{u}\mathbf{\Gamma}_\mu^{\text{V-A}} s|\Lambda\rangle \cdot \langle \ell\bar{\nu}_\ell|\bar{\ell}\mathbf{\Gamma}_\mu^{\text{V-A}}\nu_\ell|0\rangle, \quad (1)$$

where $\mathbf{\Gamma}_\mu^{\text{V-A}} = \gamma_\mu(1-\gamma_5)$ is the left-handed operator representing in the standard model the weak coupling between left-handed fermions. Two components in this expression are well known: the Fermi constant, G_F, which is determined from muon decay [1], and the leptonic matrix elements, $\langle \ell\bar{\nu}_\ell|\bar{\ell}\mathbf{\Gamma}_\mu^{\text{V-A}}\nu_\ell|0\rangle$, which are computed perturbatively. The remaining two components are less known and constitute the central focus of this Letter: (1) the hadronic matrix element $\langle p|\bar{u}\mathbf{\Gamma}_\mu^{\text{V-A}} s|\Lambda\rangle$ encodes the nonperturbative QCD dynamics governing the transition of a Λ hyperon into a proton. It is conventionally expressed in terms of six form factors, which encapsulate the effects of strong interactions. While previous phenomenological studies have extracted these form factors using a combination of experimental data, effective models, and symmetry arguments, first-principles calculations from lattice QCD have not been performed prior to this Letter for this particular decay. (2) The Cabibbo-Kobayashi-Maskawa (CKM) matrix element V_{us}—related to the Cabibbo angle by $V_{us} \equiv \sin(\theta_{\text{Cabibbo}})$—governs the strength of weak transitions between strange and up quarks through its magnitude $|V_{us}|$. Currently, this value exhibits a tension among different approaches used for its determination, such as extractions from kaon and tau decays, as well as from the CKM first-row unitarity relation [2]. Given this discrepancy, independent determinations of $|V_{us}|$ are of critical importance.

Semileptonic hyperon decays, such as $\Lambda \to p\ell\bar{\nu}_\ell$, offer an alternative and complementary approach to extracting $|V_{us}|$, as first studied by Cabibbo *et al.* in Refs. [3,4]. However, due to the absence of updated experimental measurements and nonperturbative theoretical calculations, this two-decade-old result remains the state-of-the-art determination from hyperons [2]. By providing a first-principles lattice QCD determination of the $\Lambda \to N$ form factors, this Letter establishes the basis for a more precise and accurate extraction of $|V_{us}|$ from hyperon decays. The calculation is performed on a single gauge ensemble generated at physical light, strange, and charm quark masses by the ETM Collaboration. This Letter clearly demonstrates that lattice QCD can compute the relevant

Published by the American Physical Society under the terms of the Creative Commons Attribution 4.0 International license. Further distribution of this work must maintain attribution to the author(s) and the published article's title, journal citation, and DOI. Funded by SCOAP³.

matrix elements with sufficient precision to enable a fully controlled, nonperturbative determination of $|V_{us}|$ from hyperon decays.

This Letter aligns with current experimental efforts to measure the semileptonic decay $\Lambda \to p\ell\bar{\nu}_\ell$ at BESIII and LHCb. While previous hyperon decay studies [2] focused solely on the decay process, excluding the production mechanism, BESIII's ability to reconstruct the full baryon-antibaryon ($B\bar{B}$) pair enables a novel approach that incorporates the production process [5]. This allows simultaneous modeling of the joint angular distributions of production and decay, providing additional observables in various kinematic regions to compare with theoretical predictions. Furthermore, a comparison between first-principles standard model calculations and experimental measurements provides constraints on nonstandard interactions [6–8]. Deviations in the axial coupling may signal nonzero right-handed currents, while discrepancies in the ratio of the muon to electron channel decay rate, $\Gamma(\Lambda \to p\mu\bar{\nu}_\mu)/\Gamma(\Lambda \to pe\bar{\nu}_e)$, may indicate scalar and/or tensor contributions [8].

Theoretical formalism—The rate Γ of the semileptonic decay $\Lambda \to p\ell\bar{\nu}_\ell$ can be computed as an integral over the final-state phase space,

$$\Gamma = \frac{1}{2m_\Lambda}\int \frac{d^3\vec{p}_p}{(2\pi)^3 2E_p}\frac{d^3\vec{p}_\ell}{(2\pi)^3 2E_\ell}\frac{d^3\vec{p}_\nu}{(2\pi)^3 2E_\nu} \times (2\pi)^4\delta^{(4)}(p_\Lambda - p_p - p_\ell - p_\nu)|\mathcal{M}|^2, \quad (2)$$

where $\mathcal{M}$ is the invariant matrix element defined in Eq. (1), p is the four-momentum, and $E = \sqrt{m^2 + |\vec{p}|^2}$ are the energies of the initial and final particles of mass m. Integrating out the angular variables leads to a dependence only on the squared momentum transfer $q^2 = (p_\Lambda - p_p)^2 = (p_\ell + p_\nu)^2$, which corresponds to the invariant mass squared of the lepton-neutrino system. The decay rate then reduces to

$$\Gamma = \frac{G_F^2|V_{us}|^2}{192\pi^3 m_\Lambda^3}\int_{m_\ell^2}^{q^2_{\max}} dq^2\sqrt{\lambda(m_\Lambda^2, m_p^2, q^2)}L^{\mu\nu}H_{\mu\nu}, \quad (3)$$

where $q^2_{\max} = (m_\Lambda - m_p)^2$ is the maximum allowed momentum transfer, $\lambda(a,b,c) = a^2 + b^2 + c^2 - 2(ab + bc + ca)$ is the Källén function, and $L^{\mu\nu}$ and $H_{\mu\nu}$ are the leptonic and hadronic tensors, respectively. The latter, arising from the angular integration of $|\mathcal{M}|^2$, are given by

$$L^{\mu\nu} \equiv \left(1 - \frac{m_\ell^2}{q^2}\right)^2\left[\frac{q^\mu q^\nu}{q^2}\left(1 + \frac{m_\ell^2}{2q^2}\right) - g^{\mu\nu}\right], \quad (4)$$

$$H_{\mu\nu} \equiv \sum_{s_p, s_\Lambda} M_\mu^{\text{V-A}}(M_\nu^{\text{V-A}})^*, \quad (5)$$

where $g_{\mu\nu} = \text{diag}(+,-,-,-)$ is the Minkowski metric, s_p, s_Λ are the spins of the baryons, and the hadronic matrix element $M_\mu^{\text{V-A}}$ is defined as

$$M_\mu^{\text{V-A}} \equiv \langle p(p_p, s_p)|\bar{u}\mathbf{\Gamma}_\mu^{\text{V-A}}s|\Lambda(p_\Lambda, s_\Lambda)\rangle. \quad (6)$$

From matrix elements to form factors: The hadronic matrix elements are expressed in terms of Lorentz-invariant form factors, which provide a general decomposition consistent with the symmetries of QCD and depend only on the momentum transfer q^2. In this Letter, we use both the Weinberg [9] and helicity [10] formalisms: the former is standard in phenomenological analyses, while the latter is better suited for computing the decay rate, as it maps directly onto angular distributions and polarization observables. The decomposition of the matrix elements in the Weinberg basis and Minkowski space is given by

$$M_\mu^{\text{V-A}} = \bar{u}_p\Big[\gamma_\mu(F_1(q^2) - G_1(q^2)\gamma_5) - i\sigma_{\mu\nu}q^\nu\frac{F_2(q^2) - G_2(q^2)\gamma_5}{m_\Lambda} + q_\mu\frac{F_3(q^2) - G_3(q^2)\gamma_5}{m_\Lambda}\Big]u_\Lambda, \quad (7)$$

where $\sigma^{\mu\nu} = (i/2)[\gamma^\mu, \gamma^\nu]$ is the antisymmetric tensor Dirac matrix and u_Λ, u_p are spinors defined as

$$u_B \equiv \frac{\not{p}_B + m_B}{\sqrt{2E_B(E_B + m_B)}}u^s \quad (8)$$

for $B \in \{p, \Lambda\}$, with u^s being an up- or down-spin state.

The form factors $F_1(q^2), F_2(q^2)$, and $F_3(q^2)$ originate from the vector current $V_\mu = \bar{u}\gamma_\mu s$, while $G_1(q^2), G_2(q^2)$, and $G_3(q^3)$ arise from the axial-vector current $A_\mu = \bar{u}\gamma_\mu\gamma_5 s$. $F_1(q^2)$ and $F_2(q^2)$ are known as the Dirac and Pauli form factors, and $G_1(q^2)$ and $G_3(q^2)$ as the axial and induced pseudoscalar form factors—structures also present in diagonal matrix elements. In contrast, $F_3(q^2)$ and $G_2(q^2)$ are second-class form factors [11]: they are proportional to the mass splitting and vanish in the exact SU(3) flavor symmetry limit, where the quark masses are degenerate and $m_p = m_\Lambda$. Additionally, both $F_3(q^2)$ and $G_3(q^2)$ contribute to the decay rate only through terms suppressed by m_ℓ^2. As a result, $F_3(q^2)$ is negligible in all channels at the targeted precision, while $G_3(q^2)$ becomes relevant only in the muonic mode, since m_μ is similar in size to the mass splitting.

Further details on the theoretical formalism are provided in the End Matter, including the definitions of the helicity form factors, the relations between Weinberg and helicity, the expression for the decay rate once the leptonic and hadronic tensors are contracted, and the perturbative approximation of the decay rate at leading orders of the mass splitting.

Lattice QCD methodology—Lattice QCD provides a nonperturbative framework for studying the strong

interaction by discretizing the QCD Lagrangian on a four-dimensional Euclidean spacetime lattice. This enables *ab initio* numerical simulations that incorporate the full dynamics of QCD with controlled and systematically improvable uncertainties. In the past decade, lattice QCD has reached high precision across a wide range of observables and extended into regimes previously out of reach. Of particular relevance to this Letter are precise lattice results on nucleon structure, including isovector charges [12–17], axial form factors [17–19], and electromagnetic form factors [20–22]. These advances reflect significant progress in controlling key systematics, including excited-state contamination, discretization effects, and simulations at the physical quark masses.

The lattice approach is especially well suited for studying semileptonic baryon decays via form factor determinations, as demonstrated in several prior calculations: $\Lambda_b \to N, \Lambda_c$ [23], $\Lambda_c \to \Lambda$ [24], $\Lambda_c \to N$ [25], $\Lambda_c \to \Lambda^{(1520)}$ [26], $\Lambda_b \to \Lambda_c^{(2595,2625)}$ [27], and $\Xi_c \to \Xi$ [28]. In contrast, lattice QCD results for hyperon transitions remain sparse, limited to the vector form factor $F_1(q^2)$ in $\Sigma \to N$ and $\Xi \to \Sigma$ transition [29,30], or to early studies of form factors performed at heavier-than-physical pion masses for the $\Xi \to \Sigma$ transition [31]. The present Letter represents a significant step forward, extending the scope and phenomenological impact of lattice studies of hyperon semileptonic decays.

Simulation setup: We analyze a gauge ensemble generated with light, strange, and charm quark masses set to their physical values, referred to as the "physical point." Working at the physical point eliminates the need for a chiral extrapolation in the pion mass, a significant advantage. As the aim of this Letter is to establish the theoretical framework and demonstrate that lattice QCD can achieve the precision required for an impactful determination of the form factors involved in this decay and the precise extraction of $|V_{us}|$, we perform the analysis using a single gauge ensemble with lattice spacing $a \simeq 0.08$ fm and physical volume $L \simeq 5$ fm. Lattice systematic effects related to discretization and finite volume are not addressed in this Letter. Previous studies of nucleon structure on the same ensemble [15,19,32] suggest that such effects are small, in part thanks to the use of an $\mathcal{O}(a)$-improved action. Nevertheless, we plan to quantify these effects in future work to provide a complete error budget. The simulations are performed in the SU(2)-isosymmetric limit, where up and down quarks are degenerate, rendering the proton and neutron degenerate as well, collectively referred to as nucleons, N. Leading-order isospin-breaking, and radiative corrections are expected to be small, contributing at the (sub)percent level, and are neglected in current state-of-the-art lattice calculations of baryon matrix elements.

Interpolating fields and correlation functions: To isolate the nucleon and Λ-hyperon ground states, we employ the standard interpolating fields,

$$\chi_N(x) = \epsilon^{abc}\left(u^a(x)^T C\gamma_5 d^b(x)\right)u^c(x), \tag{9}$$

$$\begin{aligned}\chi_\Lambda(x) = \frac{1}{\sqrt{6}}\epsilon^{abc}\Big[&2\left(u_a^T(x)C\gamma_5 d^b(x)\right)s^c(x)\\ &+\left(u^a(x)^T C\gamma_5 s^b(x)\right)d^c(x)\\ &-\left(d^a(x)^T C\gamma_5 s^b(x)\right)u^c(x)\Big],\end{aligned} \tag{10}$$

where u, d, and s denote the up-, down-, and strange-quark spinors at the spacetime point $x \equiv (\vec{x}, t)$, C is the charge conjugation matrix, and a, b, c are implicitly summed color indices. We construct two-point correlation functions as

$$C_B(\vec{p}_B, t_s) = \sum_{\vec{x}_s}\mathrm{Tr}[P_0\langle\chi_B(x_s)\bar{\chi}_B(0)\rangle e^{-i\vec{x}_s\cdot\vec{p}_B}] \tag{11}$$

for $B \in \{N, \Lambda\}$, where the trace is taken over the implicit Dirac indices of the interpolating fields, and the $\Lambda \to N$ transition three-point correlation function as

$$\begin{aligned}&C_\mu^{\text{V-A}}(\vec{p}_N, \vec{p}_\Lambda, t_s, t_{\text{ins}})\\ &\quad= \sum_{\vec{x}_{\text{ins}}, \vec{x}_s} e^{i\vec{x}_{\text{ins}}\cdot(\vec{p}_\Lambda - \vec{p}_N) - i\vec{x}_s\cdot\vec{p}_\Lambda}\\ &\qquad\times \mathrm{Tr}\left[P_\nu\langle\chi_\Lambda(x_s)\bar{u}(x_{\text{ins}})\mathbf{\Gamma}_\mu^{\text{V-A}} s(x_{\text{ins}})\bar{\chi}_N(0)\rangle\right].\end{aligned} \tag{12}$$

Here, x_s and x_{ins} denote the spacetime coordinates of the Λ annihilation (sink) and current insertion, respectively, relatively to the spacetime of the creation of the nucleon (source) taken, without loss of generality, at zero. Two-point functions are Fourier-transformed at the sink to access various momenta $\vec{p}_B$, while three-point functions are constructed using the fixed-sink method at fixed t_s and sink momentum $\vec{p}_\Lambda = \vec{0}$, and Fourier-transformed with respect to the momentum transfer, $\vec{q}$. P_ν is a projector, which acts on spin indices. For unpolarized matrix elements with positive parity we use $P_0 = \frac{1}{2}(1 + \gamma_0)$, while for polarized matrix elements we use $P_k = iP_0\gamma_5\gamma_k$.

Extraction of ground-state matrix elements: Matrix elements are extracted from appropriately defined ratios of two- and three-point functions that cancel both the overlap factors between interpolating fields and hadron states, and exponential time dependencies. We use

$$R_{\mu\nu}^{\text{V-A}}(\vec{p}_N, \vec{p}_\Lambda, t_s, t_{\text{ins}}) \equiv \frac{C_{\mu\nu}^{\text{V-A}}(\vec{p}_N, \vec{p}_\Lambda, t_s, t_{\text{ins}})}{\sqrt{C_\Lambda(\vec{p}_\Lambda, t_s)C_N(\vec{p}_N, t_s)}}. \tag{13}$$

In the limit of large time separations, $t_s \gg a$, and for operator insertion at $t_{\text{ins}} = t_s/2$, the ratio becomes time-independent,

$$R_{\mu\nu}^{\text{V-A}}(\vec{p}_N, \vec{p}_\Lambda, t_s, t_s/2) \xrightarrow[t_s \gg a]{} \Pi_{\mu\nu}^{\text{V-A}}(\vec{p}_N, \vec{p}_\Lambda), \tag{14}$$

obtaining matrix elements like those defined in Eq. (7), but for a given polarization P_ν and momentum choice.

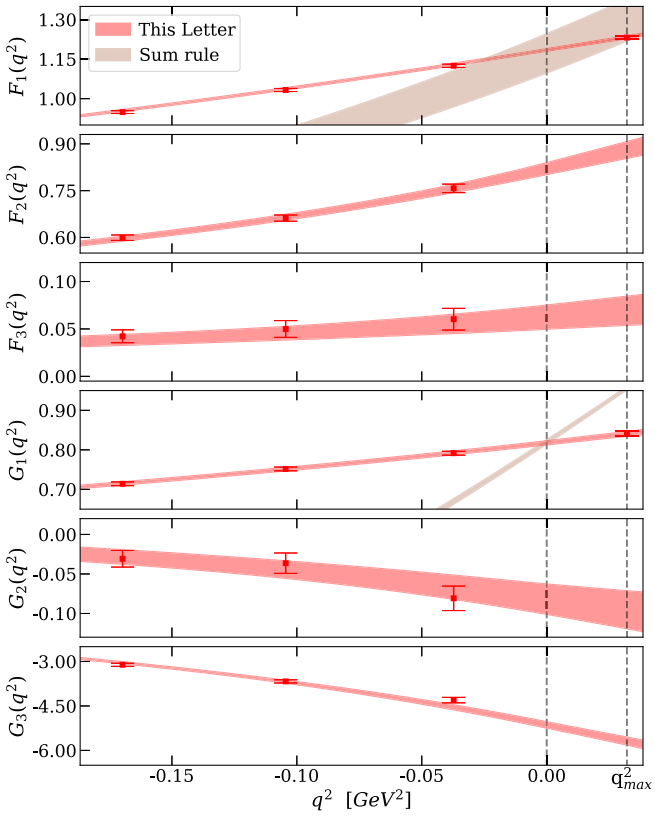


FIG. 1. Momentum transfer dependence of the Weinberg form factors. Red points denote selected lattice data. The red band represents the z-expansion fit, while the brown band shows results from QCD sum rules [54]. Vertical dashed lines indicate the kinematic region relevant for the semileptonic decay rate, $q^2 \in [0, q^2_{\rm max}]$.

Form factors are extracted from linear combinations of $\Pi^{\rm V\text{-}A}_{\mu\nu}(\vec{p}_N, \vec{p}_\Lambda)$. A critical aspect of reliably determining ground-state matrix elements is controlling excited-state contamination. Achieving ground-state dominance is hindered by the rapid growth of statistical noise with increasing source-sink separation t_s. To mitigate this, we employ multiple strategies, including the summation method and two-state fits to model the time dependence of the ration in Eq. (13) and determine its asymptotic behavior. The full extraction procedure, along with a detailed account of the systematics, is provided in Supplemental Material [33].

Results—

Weinberg form factors and couplings: In Fig. 1, we show our final results for the Weinberg form factors. For the $F_1(q^2)$ and $G_1(q^2)$ form factors, we compare against QCD sum rule results from Ref. [54]. While the couplings, i.e., the form factors at $q^2 = 0$, agree well, we observe tension in the q^2 dependence. In Fig. 2, we compare commonly used coupling ratios with experimental data and phenomenological analyses. We find good agreement with the results of PDG and QCD sum rules, notably achieving a significantly higher precision. Our values are

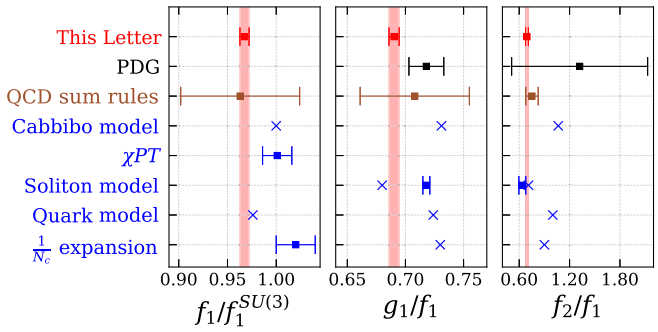


FIG. 2. Comparison of ratios of coupling constants with experimental and phenomenological ones. Points marked with a cross do not have uncertainties. The experimental values for g_1/f_1 and f_2/f_1 are taken from the Particle Data Group (PDG) [2] and are shown in black. Results from phenomenology include QCD sum rules [54], Cabibbo's model [4], chiral perturbation theory (χPT) [55], the soliton model, where points with errors are from Ref. [56] and those without from Ref. [57], the quark model, where f_1 is taken from Ref. [58], and g_1/f_1 and f_2/f_1 from Ref. [59], and the $1/N_c$ expansion [60].

$$\frac{f_1}{f_1^{\rm SU(3)}} = 0.9674(47), \quad \frac{g_1}{f_1} = 0.6902(44), \quad \frac{f_2}{f_1} = 0.693(17), \tag{15}$$

where the error is the result of model averaging over different fit ranges to extract the matrix element and $f_1^{\rm SU(3)} = \sqrt{3/2}$ is the SU(3)-flavor limit predicted by the Ademollo-Gatto theorem.

Determination of decay rates: We compute the decay rate of $\Lambda \to p\ell\bar{\nu}_\ell$ for both the electron ($\ell = e^-$) and muon ($\ell = \mu^-$) channels. Equation (3) is solved without fixing $|V_{us}|$, yielding results for $\Gamma/|V_{us}|^2$. As input, we use the leptonic masses $m_e = 0.511$ MeV and $m_\mu = 0.10566$ GeV, and the Fermi constant $G_F = 1.166\,38 \cdot (1 + 0.0105) \times 10^{-5}$ GeV^{-2} [2], where the factor $(1 + 0.0105)$ accounts for radiative corrections [61]. For the input on the baryon masses, we present two approaches: (a) Using lattice-determined values, $m_N = 0.9471(28)$ GeV and $m_\Lambda = 1.1263(23)$ GeV, yields the results in Eqs. (A14) and (A15). Although the baryon mass uncertainties are at the per-mille level, the resulting mass splitting $m_\Lambda - m_N = 0.1792(24)$ GeV carries a percent-level uncertainty. Since the decay rate scales with the fifth power of this splitting at leading order, the associated error is amplified by a factor of 5, making it the dominant source of uncertainty. (b) Using the experimental masses, $m_p^{\rm PRD} = 0.938\,27$ GeV and $m_\Lambda^{\rm PRD} = 1.115\,68$ GeV, eliminates this uncertainty, yielding the results in Eqs. (A16)–(A18). This choice illustrates the effect of using physical masses; however, on the current ensemble, we observe a percent-level discrepancy between lattice and experimental baryon masses—a known cutoff effect that vanishes in the continuum limit [62]. This leads

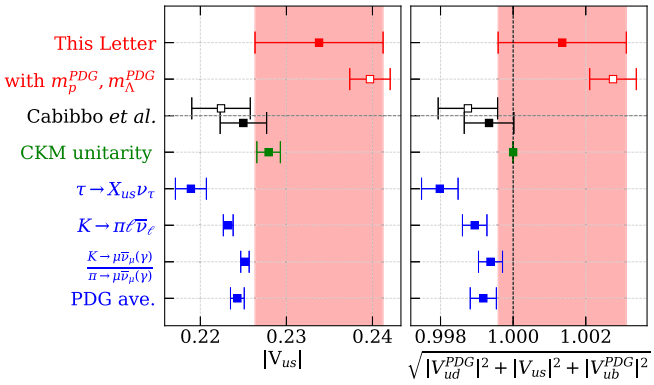


FIG. 3. Determination of V_{us} (left) and the resulting CKM unitarity relation (right). Our results are shown in red: the top one uses lattice-determined nucleon and Λ masses, approach (a), while the second one with open symbols uses PDG values, approach (b). The black points correspond to the values by Cabibbo *et al.* [4], where the empty point is the value derived from the Λ semileptonic decay, while the full point combines results from various hyperon decays. The green point is obtained from the unitarity relation. The remaining blue points show results on decay rates using lattice QCD combined with experimental data. Going from top to bottom, the first blue square is from inclusive τ decays [63], the second from kaon semileptonic decays [16,64–66], the third from the ratio of kaon to pion leptonic decays in the muonic channel [16,64,67–71], and the last is the PDG average of the latter two [2].

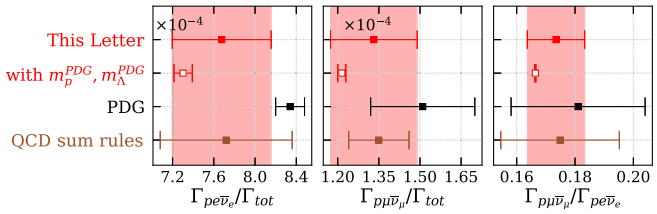


FIG. 4. Results on the decay rates in the electron and muon channels and their ratio. The notation of the red points is the same as in Fig. 3. The PDG value is shown by the black points [2] and the QCD sum rules value by the brown points [54].

to a shift in the decay rate of approximately one standard deviation relative to approach (a).

We opt to quote as final results those obtained using the baryon masses determined from the lattice analysis [approach (a)], ensuring consistency with our simulation setup. We present results from approach (b) for comparison to indicate the expected precision once the continuum-extrapolated form factors are combined with the physical masses.

Final results: A robust, $|V_{us}|$-independent prediction from our analysis is the ratio of muon to electron channel decay rates,

$$R^{\mu e} \equiv \frac{\Gamma_{p\mu\bar{\nu}_\mu}}{\Gamma_{pe\bar{\nu}_e}} = 0.1735(98). \tag{16}$$

To obtain further results, we consider two approaches: (i) using the experimental electron-channel decay rate, we extract $|V_{us}|$. Specifically, we take $\Gamma^{\rm PDG}_{pe\bar{\nu}_e} = 8.34(14) \times 10^{-4} \times \Gamma^{\rm PDG}_{\rm tot}$ with the total decay rate $\Gamma^{\rm PDG}_{\rm tot} = 1/\tau^{\rm PDG}_\Lambda$ and the Λ lifetime $\tau^{\rm PDG}_\Lambda = 2.617(10) \times 10^{-10}$ s, yielding

$$|V_{us}| \equiv \left(\frac{\Gamma_{pe\bar{\nu}_e}}{|V_{us}|^2}\frac{1}{\Gamma^{\rm PDG}_{pe\bar{\nu}_e}}\right)^{-1/2} = 0.2338(75), \tag{17}$$

$$\sqrt{|V^{\rm PDG}_{ud}|^2 + |V_{us}|^2 + |V^{\rm PDG}_{ub}|^2} = 1.0014(18), \tag{18}$$

where the second relation tests first-row CKM unitarity, expected to equal unity in the standard model, using $|V^{\rm PDG}_{ud}| = 0.973\,67(32)$ and $|V^{\rm PDG}_{ub}| = 3.82(20) \times 10^{-3}$ [2]. A comparison of these results with other determinations is shown in Fig. 3. (ii) Alternatively, using as input the PDG average value $|V^{\rm PDG}_{us}| = 0.2243(8)$—extracted from semileptonic and leptonic Kaon decays—we obtain

$$\frac{\Gamma_{pe\bar{\nu}_e}}{\Gamma_{\rm tot}} \equiv \frac{\Gamma_{pe\bar{\nu}_e}}{|V_{us}|^2}\frac{|V^{\rm PDG}_{us}|^2}{\Gamma^{\rm PDG}_{\rm tot}} = 7.68(48) \times 10^{-4}, \tag{19}$$

$$\frac{\Gamma_{p\mu\bar{\nu}_\mu}}{\Gamma_{\rm tot}} \equiv \frac{\Gamma_{p\mu\bar{\nu}_\mu}}{|V_{us}|^2}\frac{|V^{\rm PDG}_{us}|^2}{\Gamma^{\rm PDG}_{\rm tot}} = 1.33(16) \times 10^{-4}. \tag{20}$$

A comparison of these results is shown in Fig. 4, including the ratio of the two channels.

Conclusions—We have presented the first lattice QCD calculation of the vector and axial-vector form factors governing the semileptonic decay $\Lambda \to p\ell\bar{\nu}_\ell$. These form factors are critical for probing the weak structure of hyperons and provide an independent avenue for determining the CKM matrix element $|V_{us}|$. Our calculation is performed on a single gauge-field ensemble with physical-mass up, down, strange, and charm quarks, eliminating the need for a chiral extrapolation. Discretization effects will be investigated in future studies but are expected to remain within the quoted uncertainties of our final results, based on corresponding results in the nucleon sector using the present ensemble and others at finer lattice spacings [19,22].

Our results for the form factor couplings are consistent with theoretical expectations, phenomenological models, and available experimental data. By integrating the differential decay rate over the full kinematic range, we obtain the partial decay rates for both electron and muon channels in units of $|V_{us}|^2$. This yields a precise lattice QCD prediction for their ratio, Eq. (16), and a new determination of $|V_{us}|$, Eq. (19), when the experimental decay rate of the electron channel is used as input.

The ratio computed from lattice QCD is significantly more precise than current experimental averages and is consistent with them, thereby ruling out the presence of scalar or tensor nonstandard interactions at the current level of sensitivity [8]. Our determination of $|V_{us}|$ is consistent with CKM unitarity, albeit with a larger uncertainty than other determinations that show a notable tension. Compared to the phenomenological estimate from hyperon decays by Cabibbo *et al.* [4], we find that the

approximations used in that analysis—such as substituting f_1 with $f_1^{\mathrm{SU}(3)}$, neglecting second-class form factors, and ignoring the q^2 dependence—introduce systematic effects of a few percent. In particular, we find that neglecting the q^2 dependence leads to a 3.6(3)% deviation in the electron-mode decay rate, while using the next-to-next-to-leading order in Eq. (A20), which incorporates q^2 dependence through the radii, results in a deviation of -1%, as reported in Eq. (A21). This highlights the need for a nonperturbative approach, such as the present Letter, to achieve a sub-percent accuracy in the determination of $|V_{us}|$.

Ensemble generation employed the open-source packages tmLQCD [72–75], DD-αAMG [76–79], and QUDA [80–82]. Analysis utilized the open-source software PLEGMA and QUDA.

Acknowledgments—We thank Constantia Alexandrou for her insightful comments and mentorship as A. K.'s Ph.D. advisor. We also thank the members of the ETM Collaboration for their constructive cooperation. S. B. acknowledges support from "POST-DOC/0524/0001" and "VISION ERC—PATH 2/0524/0001," cofinanced by the European Regional Development Fund and the Republic of Cyprus through the Research and Innovation Foundation within the framework of the Cohesion Policy Programme "THALIA 2021-2027." A. K. acknowledges financial support from "The three-dimensional structure of the nucleon from lattice QCD" 3D-N-LQCD program, funded by the University of Cyprus. We gratefully acknowledge the Gauss Centre for Supercomputing e.V. ([83]) for computing time on JUWELS Booster at the Jülich Supercomputing Centre (JSC). We also acknowledge the Swiss National Supercomputing Centre (CSCS) and the EuroHPC Joint Undertaking for access to the Daint-Alps supercomputer. We are grateful to CINECA and the EuroHPC JU for access to the supercomputing facilities hosted at CINECA and Leonardo-Booster.

Data availability—The data that support the findings of this article are not publicly available upon publication because it is not technically feasible and/or the cost of preparing, depositing, and hosting the data would be prohibitive within the terms of this research project. The data are available from the authors upon reasonable request.

[1] D. B. Chitwood *et al.* (MuLan Collaboration), Phys. Rev. Lett. **99**, 032001 (2007).
[2] S. Navas *et al.* (Particle Data Group), Phys. Rev. D **110**, 030001 (2024).
[3] N. Cabibbo, E. C. Swallow, and R. Winston, Phys. Rev. Lett. **92**, 251803 (2004).
[4] N. Cabibbo, E. C. Swallow, and R. Winston, Annu. Rev. Nucl. Part. Sci. **53**, 39 (2003).
[5] V. Batozskaya, A. Kupsc, N. Salone, and J. Wiechnik, Phys. Rev. D **108**, 016011 (2023).
[6] V. Cirigliano, J. Jenkins, and M. Gonzalez-Alonso, Nucl. Phys. **B830**, 95 (2010).
[7] V. Cirigliano, M. Gonzalez-Alonso, and M. L. Graesser, J. High Energy Phys. 02 (2013) 046.
[8] H.-M. Chang, M. González-Alonso, and J. Martin Camalich, Phys. Rev. Lett. **114**, 161802 (2015).
[9] T. Gutsche, M. A. Ivanov, J. G. Körner, V. E. Lyubovitskij, and P. Santorelli, Phys. Rev. D **90**, 114033 (2014); **94**, 059902(E) (2016).
[10] T. Feldmann and M. W. Y. Yip, Phys. Rev. D **85**, 014035 (2012); **86**, 079901(E) (2012).
[11] S. Weinberg, Phys. Rev. **112**, 1375 (1958).
[12] A. Walker-Loud *et al.*, Proc. Sci. CD2018 (**2020**) 020 [arXiv:1912.08321].
[13] G. S. Bali, S. Collins, S. Heybrock, M. Löffler, R. Rödl, W. Söldner, and S. Weishäupl (RQCD Collaboration), Phys. Rev. D **108**, 034512 (2023).
[14] D. Djukanovic, G. von Hippel, H. B. Meyer, K. Ottnad, and H. Wittig, Phys. Rev. D **109**, 074507 (2024).
[15] C. Alexandrou, S. Bacchio, J. Finkenrath, C. Iona, G. Koutsou, Y. Li, and G. Spanoudes, Phys. Rev. D **111**, 054505 (2025).
[16] Y. Aoki *et al.* (Flavour Lattice Averaging Group (FLAG) Collaboration), arXiv:2411.04268.
[17] Y.-C. Jang, R. Gupta, T. Bhattacharya, B. Yoon, and H.-W. Lin (Precision Neutron Decay Matrix Elements (PNDME) Collaboration), Phys. Rev. D **109**, 014503 (2024).
[18] D. Djukanovic, G. von Hippel, J. Koponen, H. B. Meyer, K. Ottnad, T. Schulz, and H. Wittig, Phys. Rev. D **106**, 074503 (2022).
[19] C. Alexandrou, S. Bacchio, M. Constantinou, J. Finkenrath, R. Frezzotti, B. Kostrzewa, G. Koutsou, G. Spanoudes, and C. Urbach (Extended Twisted Mass Collaboration), Phys. Rev. D **109**, 034503 (2024).
[20] D. Djukanovic, G. von Hippel, H. B. Meyer, K. Ottnad, M. Salg, and H. Wittig, Phys. Rev. D **109**, 094510 (2024).
[21] R. Tsuji, Y. Aoki, K.-I. Ishikawa, Y. Kuramashi, S. Sasaki, K. Sato, E. Shintani, H. Watanabe, and T. Yamazaki (PACS Collaboration), Phys. Rev. D **109**, 094505 (2024).
[22] C. Alexandrou, S. Bacchio, G. Koutsou, B. Prasad, and G. Spanoudes, arXiv:2507.20910.
[23] W. Detmold, C. Lehner, and S. Meinel, Phys. Rev. D **92**, 034503 (2015).
[24] S. Meinel, Phys. Rev. Lett. **118**, 082001 (2017).
[25] S. Meinel, Phys. Rev. D **97**, 034511 (2018).
[26] S. Meinel and G. Rendon, Phys. Rev. D **105**, 054511 (2022).
[27] S. Meinel and G. Rendon, Phys. Rev. D **103**, 094516 (2021).
[28] C. Farrell and S. Meinel, Phys. Rev. D **111**, 114521 (2025).
[29] P. E. Shanahan, A. N. Cooke, R. Horsley, Y. Nakamura, P. E. L. Rakow, G. Schierholz, A. W. Thomas, R. D. Young, and J. M. Zanotti, Phys. Rev. D **92**, 074029 (2015).
[30] S. Sasaki, Phys. Rev. D **96**, 074509 (2017).
[31] S. Sasaki and T. Yamazaki, Phys. Rev. D **79**, 074508 (2009).
[32] C. Alexandrou, S. Bacchio, G. Koutsou, B. Prasad, and G. Spanoudes, Proc. Sci. LATTICE2024 (**2025**) 332 [arXiv:2502.11301].
[33] See Supplemental Material at http://link.aps.org/supplemental/10.1103/bvs9-wcsj for details on the generation and analysis of lattice QCD data, which includes Refs. [34–53].

[34] R. Frezzotti, P. A. Grassi, S. Sint, and P. Weisz (Alpha Collaboration), J. High Energy Phys. 08 (2001) 058.
[35] R. Frezzotti and G. C. Rossi, J. High Energy Phys. 08 (2004) 007.
[36] B. Sheikholeslami and R. Wohlert, Nucl. Phys. **B259**, 572 (1985).
[37] C. Alexandrou *et al.*, Phys. Rev. D **98**, 054518 (2018).
[38] J. Finkenrath *et al.*, Proc. Sci. LATTICE2021 (**2022**) 284 [arXiv:2201.02551].
[39] C. Alexandrou *et al.* (Extended Twisted Mass Collaboration), Phys. Rev. D **107**, 074506 (2023).
[40] C. Alexandrou *et al.* (Extended Twisted Mass Collaboration), Phys. Rev. D **104**, 074515 (2021).
[41] C. Alexandrou *et al.* (Extended Twisted Mass Collaboration), Phys. Rev. D **111**, 054502 (2025).
[42] S. Gusken, U. Low, K. H. Mutter, R. Sommer, A. Patel, and K. Schilling, Phys. Lett. B **227**, 266 (1989).
[43] C. Alexandrou, S. Gusken, F. Jegerlehner, K. Schilling, and R. Sommer, Nucl. Phys. **B414**, 815 (1994).
[44] M. Albanese *et al.* (APE Collaboration), Phys. Lett. B **192**, 163 (1987).
[45] O. Bar, Phys. Rev. D **99**, 054506 (2019).
[46] Y.-C. Jang, R. Gupta, B. Yoon, and T. Bhattacharya, Phys. Rev. Lett. **124**, 072002 (2020).
[47] C. Alexandrou, M. Constantinou, S. Dinter, V. Drach, K. Jansen, C. Kallidonis, and G. Koutsou, Phys. Rev. D **88**, 014509 (2013).
[48] C. Alexandrou, M. Brinet, J. Carbonell, M. Constantinou, P. A. Harraud, P. Guichon, K. Jansen, T. Korzec, and M. Papinutto, Phys. Rev. D **83**, 094502 (2011).
[49] C. Alexandrou, G. Koutsou, J. W. Negele, and A. Tsapalis, Phys. Rev. D **74**, 034508 (2006).
[50] L. Maiani, G. Martinelli, M. L. Paciello, and B. Taglienti, Nucl. Phys. **B293**, 420 (1987).
[51] S. Capitani, M. Della Morte, G. von Hippel, B. Jager, A. Juttner, B. Knippschild, H. B. Meyer, and H. Wittig, Phys. Rev. D **86**, 074502 (2012).
[52] W. I. Jay and E. T. Neil, Phys. Rev. D **103**, 114502 (2021).
[53] E. T. Neil and J. W. Sitison, Phys. Rev. D **109**, 014510 (2024).
[54] S.-Q. Zhang, X.-H. Zhang, and C.-F. Qiao, J. High Energy Phys. 06 (2024) 122.
[55] L. S. Geng, J. Martin Camalich, and M. J. Vicente Vacas, Phys. Rev. D **79**, 094022 (2009).
[56] G.-S. Yang and H.-C. Kim, Phys. Rev. C **92**, 035206 (2015).
[57] T. Ledwig, A. Silva, H.-C. Kim, and K. Goeke, J. High Energy Phys. 07 (2008) 132.
[58] F. Schlumpf, Phys. Rev. D **51**, 2262 (1995).
[59] A. Faessler, T. Gutsche, B. R. Holstein, M. A. Ivanov, J. G. Korner, and V. E. Lyubovitskij, Phys. Rev. D **78**, 094005 (2008).
[60] R. Flores-Mendieta, E. E. Jenkins, and A. V. Manohar, Phys. Rev. D **58**, 094028 (1998).
[61] A. Garcia and P. Kielanowski, *The Beta Decay of Hyperons*, edited by A. Bohm (Springer, Berlin, Heidelberg, 1985), Vol. 222.
[62] C. Alexandrou, S. Bacchio, G. Christou, and J. Finkenrath, Phys. Rev. D **108**, 094510 (2023).
[63] C. Alexandrou *et al.* (Extended Twisted Mass Collaboration), Phys. Rev. Lett. **132**, 261901 (2024).
[64] M. Moulson, Proc. Sci. CKM2016 (**2017**) 033 [arXiv:1704.04104].
[65] N. Carrasco, P. Lami, V. Lubicz, L. Riggio, S. Simula, and C. Tarantino, Phys. Rev. D **93**, 114512 (2016).
[66] A. Bazavov *et al.* (Fermilab Lattice and MILC Collaborations), Phys. Rev. D **99**, 114509 (2019).
[67] R. J. Dowdall, C. T. H. Davies, G. P. Lepage, and C. McNeile, Phys. Rev. D **88**, 074504 (2013).
[68] N. Carrasco *et al.*, Phys. Rev. D **91**, 054507 (2015).
[69] A. Bazavov *et al.*, Phys. Rev. D **98**, 074512 (2018).
[70] N. Miller *et al.*, Phys. Rev. D **102**, 034507 (2020).
[71] C. Alexandrou *et al.* (Extended Twisted Mass Collaboration), Phys. Rev. D **104**, 074520 (2021).
[72] K. Jansen and C. Urbach, Comput. Phys. Commun. **180**, 2717 (2009).
[73] A. Abdel-Rehim, F. Burger, A. Deuzeman, K. Jansen, B. Kostrzewa, L. Scorzato, and C. Urbach, Proc. Sci. LATTICE2013 (**2014**) 414 [arXiv:1311.5495].
[74] A. Deuzeman, K. Jansen, B. Kostrzewa, and C. Urbach, Proc. Sci. LATTICE2013 (**2014**) 416 [arXiv:1311.4521].
[75] B. Kostrzewa, S. Bacchio, J. Finkenrath, M. Garofalo, F. Pittler, S. Romiti, and C. Urbach (ETM Collaboration), Proc. Sci. LATTICE2022 (**2023**) 340 [arXiv:2212.06635].
[76] A. Frommer, K. Kahl, S. Krieg, B. Leder, and M. Rottmann, SIAM J. Sci. Comput. **36**, A1581 (2014).
[77] C. Alexandrou, S. Bacchio, J. Finkenrath, A. Frommer, K. Kahl, and M. Rottmann, Phys. Rev. D **94**, 114509 (2016).
[78] S. Bacchio, C. Alexandrou, and J. Finkerath, EPJ Web Conf. **175**, 02002 (2018).
[79] C. Alexandrou, S. Bacchio, and J. Finkenrath, Comput. Phys. Commun. **236**, 51 (2019).
[80] M. A. Clark, R. Babich, K. Barros, R. C. Brower, and C. Rebbi (QUDA Collaboration), Comput. Phys. Commun. **181**, 1517 (2010).
[81] R. Babich, M. A. Clark, B. Joo, G. Shi, R. C. Brower, and S. Gottlieb (QUDA Collaboration), in *International Conference for High Performance Computing, Networking, Storage and Analysis* (IEEE, Seattle, Washington, USA, 2011).
[82] M. A. Clark, B. Joó, A. Strelchenko, M. Cheng, A. Gambhir, and R. C. Brower (QUDA Collaboration), in *International Conference for High Performance Computing, Networking, Storage and Analysis* (IEEE, Salt Lake City, Utah, USA, 2016).
[83] http://www.gauss-centre.eu.
[84] R. J. Hill and G. Paz, Phys. Rev. D **82**, 113005 (2010).

End Matter

Appendix—We present additional details on the theoretical formalism and the extraction of final results. The generation and analysis of the lattice QCD data are discussed separately in Supplemental Material [33].

Helicity form factors: The helicity form factors are related to the Weinberg form factors via

$$F_+(q^2) = F_1(q^2) + \frac{q^2}{m_\Lambda(m_\Lambda + m_N)} F_2(q^2), \tag{A1}$$

$$F_\perp(q^2) = F_1(q^2) + \frac{m_\Lambda + m_N}{m_\Lambda} F_2(q^2), \tag{A2}$$

$$F_0(q^2) = F_1(q^2) + \frac{q^2}{m_\Lambda(m_\Lambda - m_N)} F_3(q^2), \tag{A3}$$

$$G_+(q^2) = G_1(q^2) - \frac{q^2}{m_\Lambda(m_\Lambda - m_N)} G_2(q^2), \tag{A4}$$

$$G_\perp(q^2) = G_1(q^2) - \frac{m_\Lambda - m_N}{m_\Lambda} G_2(q^2), \tag{A5}$$

$$G_0(q^2) = G_1(q^2) - \frac{q^2}{m_\Lambda(m_\Lambda + m_N)} G_3(q^2). \tag{A6}$$

These expressions lead to the following decomposition of the matrix elements in Eq. (6) for the vector $V_\mu = \bar{u}\gamma_\mu s$ and axial-vector $A_\mu = \bar{u}\gamma_\mu\gamma_5 s$ currents, respectively:

$$\begin{aligned} M_\mu^V &= \bar{u}_p \left[\frac{(m_\Lambda - m_p)q^\mu}{q^2} F_0(q^2) + \frac{m_\Lambda + m_p}{s_+} \left(p_\Lambda^\mu + p_p^\mu - \frac{m_\Lambda^2 - m_p^2}{q^2} q^\mu \right) F_+(q^2) + \left(\gamma^\mu - \frac{2m_N p_\Lambda^\mu}{s_+} - \frac{2m_\Lambda p_p^\mu}{s_+} \right) F_\perp(q^2) \right] u_\Lambda, \\ M_\mu^A &= -\bar{u}_p\gamma_5 \left[\frac{(m_\Lambda + m_N)q^\mu}{q^2} G_0(q^2) + \frac{m_\Lambda - m_N}{s_-} \left(p_\Lambda^\mu + p_p^\mu - \frac{m_\Lambda^2 - m_N^2}{q^2} q^\mu \right) G_+(q^2) + \left(\gamma^\mu + \frac{2m_N p_\Lambda^\mu}{s_-} - \frac{2m_\Lambda p_p^\mu}{s_-} \right) G_\perp(q^2) \right] u_\Lambda. \end{aligned} \tag{A7}$$

with $s_\pm = (m_\Lambda \pm m_N)^2 - q^2$. We also note that, at $q^2 = 0$, the helicity form factors satisfy

$$F_+(0) = F_1(0) = F_0(0) \quad \text{and} \quad G_+(0) = G_1(0) = G_0(0), \tag{A8}$$

while, at the kinematic endpoint $q^2_{\max} = (m_\Lambda - m_N)^2$,

$$G_+(q^2_{\max}) = G_1(q^2_{\max}) - \frac{q^2_{\max}}{m_\Lambda} G_2(q^2_{\max}) = G_\perp(q^2_{\max}) \tag{A9}$$

holds. These constraints are imposed in our parametrization of the form factors during the analysis.

Parametrization of the q^2 dependence: Since the relevant momentum transfer region for the $\Lambda \to p$ semileptonic decay lies entirely within the low-q^2 range, approximately within $[0, 0.03]\ \mathrm{GeV}^2$, a leading-order expansion in q^2 is sufficient to determine the decay rate with subpercent precision. To this end, we define the axial-vector charges and radii as

$$g_i = G_i(0) \quad \text{and} \quad \langle r^2_{G_i} \rangle = \frac{6}{g_i} \frac{\partial G_i(q^2)}{\partial q^2}\bigg|_{q^2=0}, \tag{A10}$$

and analogously for the vector form factors by substituting $G \leftrightarrow F$ and $g \leftrightarrow f$. These definitions yield the leading low-q^2 expansion

$$G_i(q^2) = g_i \left(1 + \frac{\langle r^2_{G_i} \rangle}{6} q^2 \right) + \mathcal{O}(q^4). \tag{A11}$$

In contrast, the lattice data cover a significantly broader kinematic range, including negative q^2 and extending up to $q^2_{\max}$ for several form factors. To parametrize the full q^2 dependence in this regime, we adopt the model-independent z expansion [84], as detailed in Supplemental Material [33].

Results on charges and radii: In Table I, we provide our results for charges and radii in the Weinberg formalism, including correlation matrices between the parameters. For convenience, in Supplemental Material [33], the same table can be found for the charges and radii of the helicity form factors.

The differential decay rate: Using the helicity form factor parametrization of the hadronic matrix element yields the following expression for the differential decay rate [25]:

$$\begin{aligned} \frac{d\Gamma}{dq^2} = {} & \frac{G_F^2 |V_{us}|^2 \sqrt{s_+ s_-}}{192\pi^3 m_\Lambda^3} \left(1 - \frac{m_\ell^2}{q^2} \right)^2 \\ & \times \left\{ \frac{3m_\ell^2}{2q^2} \left(s_- [(m_\Lambda + m_N)G_0]^2 + s_+ [(m_\Lambda - m_N)F_0]^2 \right) \right. \\ & + \frac{m_\ell^2 + 2q^2}{2q^2} \left(s_+ [(m_\Lambda - m_N)G_+]^2 \right. \\ & \left. + s_- [(m_\Lambda + m_N)F_+]^2 \right) \\ & \left. + (m_\ell^2 + 2q^2) \left(s_+ [G_\perp]^2 + s_- [F_\perp]^2 \right) \right\}, \end{aligned} \tag{A12}$$

TABLE I. Charges and radii of the Weinberg form factors and the corresponding correlation matrix. The radii are provided in units of the experimental m_Λ^2 with $m_\Lambda = 1.11568$ GeV.

f_1	f_2	f_3
1.1849(57)	0.821(19)	0.062(13)
$\langle r^2_{F_1}\rangle m^2_\Lambda$	$\langle r^2_{F_2}\rangle m^2_\Lambda$	$\langle r^2_{F_3}\rangle m^2_\Lambda$
9.50(28)	17.0(23)	24.7(68)
g_1	g_2	g_3
0.8178(55)	−0.082(19)	−5.14(11)
$\langle r^2_{G_1}\rangle m^2_\Lambda$	$\langle r^2_{G_2}\rangle m^2_\Lambda$	$\langle r^2_{G_3}\rangle m^2_\Lambda$
6.46(47)	38(14)	24.7(23)

corr.	f_1	$\langle r^2_{F_1}\rangle$	f_2	$\langle r^2_{F_2}\rangle$	f_3	$\langle r^2_{F_3}\rangle$
f_1	1.00	0.11	−0.03	−0.12	−0.50	−0.33
$\langle r^2_{F_1}\rangle$	0.11	1.00	−0.16	−0.09	−0.13	−0.20
f_2	−0.03	−0.16	1.00	0.73	0.10	0.23
$\langle r^2_{F_2}\rangle$	−0.12	−0.09	0.73	1.00	0.20	0.36
f_3	−0.50	−0.13	0.10	0.20	1.00	0.66
$\langle r^2_{F_3}\rangle$	−0.33	−0.20	0.23	0.36	0.66	1.00

corr.	g_1	$\langle r^2_{G_1}\rangle$	g_2	$\langle r^2_{G_2}\rangle$	g_3	$\langle r^2_{G_3}\rangle$
g_1	1.00	0.26	0.50	−0.05	−0.19	−0.02
$\langle r^2_{G_1}\rangle$	0.26	1.00	0.47	−0.44	−0.01	−0.30
g_2	0.50	0.47	1.00	−0.24	−0.20	−0.07
$\langle r^2_{G_2}\rangle$	−0.05	−0.44	−0.24	1.00	0.20	0.80
g_3	−0.19	−0.01	−0.20	0.20	1.00	−0.15
$\langle r^2_{G_3}\rangle$	−0.02	−0.30	−0.07	0.80	−0.15	1.00

which is integrated over the range $[m_\ell^2, q^2_{\rm max}]$ to obtain the semileptonic decay rate,

$$\Gamma = \int_{m_\ell^2}^{q^2_{\rm max}} dq^2 \frac{d\Gamma}{dq^2}. \tag{A13}$$

Figure 5 shows our determination of the differential decay rates for the electron and muon channels. For comparison, we include the QCD sum rules results from Ref. [54]. The deviation observed is likely driven by the discrepancy in the q^2 dependence, already apparent in Fig. 1.

When integrating Eq. (A12), all input parameters are precisely known except for the CKM matrix element $|V_{us}|$, which exhibits a few-percent-level tension among different determinations. As a result, we can provide a robust estimate only for the ratio $\Gamma/|V_{us}|^2$, computed for both the electron and muon channels, obtaining

$$\frac{\Gamma_{pe\bar\nu_e}}{|V_{us}|^2} = 5.83(37)\times 10^7\ \text{s}^{-1}, \tag{A14}$$

$$\frac{\Gamma_{p\mu\bar\nu_\mu}}{|V_{us}|^2} = 1.01(12)\times 10^7\ \text{s}^{-1}. \tag{A15}$$

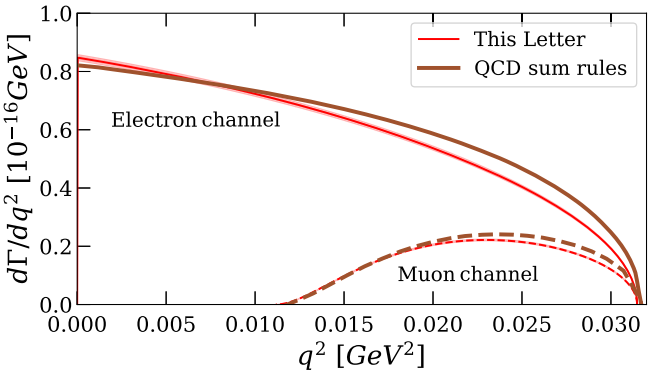


FIG. 5. Differential decay rates for the electron and muon channels. Brown lines show central values from the QCD sum rules study [54], without error bands. In contrast, our results in red include uncertainty bands. The curves are computed using $|V_{us}^{\rm PDG}| = 0.2243(8)$ for visualization purposes.

Using the experimental masses instead, we obtain

$$\frac{\Gamma_{pe\bar\nu_e}}{|V_{us}|^2} = 5.546(51)\times 10^7\ \text{s}^{-1}, \tag{A16}$$

$$\frac{\Gamma_{p\mu\bar\nu_\mu}}{|V_{us}|^2} = 0.9228(82)\times 10^7\ \text{s}^{-1}, \tag{A17}$$

$$\frac{\Gamma_{p\mu\bar\nu_\mu}}{\Gamma_{pe\bar\nu_e}} = 0.166\,38(20). \tag{A18}$$

Notably, in the latter result, the uncertainties are significantly reduced due to strong correlations between the two decay rate determinations, leading to a substantial cancellation of statistical errors.

Perturbative approximation of the decay rate: Given the narrow kinematic range, the decay rate can be computed as a perturbative expansion in the small dimensionless parameter $\delta = q_{\rm max}/m_\Lambda \approx 0.16$ and using the low-q^2 approximation of the form factors in Eq. (A11). Restricting to the electron channel, $\Lambda \to pe\bar\nu_e$, further simplifies the calculation by allowing the lepton mass to be neglected. Under these approximations, the next-to-leading order (NLO) expression for the decay rate is [4]

$$\Gamma_{\rm NLO} = \frac{G_F^2|V_{us}|^2 m_\Lambda^5 \delta^5}{60\pi^3}\left(1-\frac{3}{2}\delta\right)\left(f_1^2+3g_1^2\right). \tag{A19}$$

At next-to-next-to-leading order (NNLO), we find

$$\Gamma_{\rm NNLO} = \Gamma_{\rm NLO} + \frac{G_F^2|V_{us}|^2 m_\Lambda^5 \delta^7}{70\pi^3}\left\{f_1 f_2 + \frac{2}{3}f_2^2 - \frac{14}{3}\frac{g_1 g_2}{\delta} + f_1^2\left(1+\frac{1}{9}\langle r^2_{F_1}\rangle m^2_\Lambda\right) + g_1^2\left(2+\frac{5}{9}\langle r^2_{G_1}\rangle m^2_\Lambda\right)\right\}, \tag{A20}$$

where the $g_1 g_2/\delta$ term contributes at this order since g_2 is a second-class form factor with $g_2 \propto \delta$. Compared to the NNLO corrections given in Eq. (40) of Ref. [4], our result reinstates essential contributions proportional to the radii, arising from the q^2 dependence of the $F_1(q^2)$ and $G_1(q^2)$ form factors, which were previously omitted. When comparing to the full nonperturbative result, we find

$$\Delta_{\mathrm{NLO}} = 5.5(2)\% \quad \text{and} \quad \Delta_{\mathrm{NNLO}} = -1.14(8)\%, \tag{A21}$$

having defined $\Gamma = \Gamma_{(\mathrm{N})\mathrm{NLO}}(1 + \Delta_{(\mathrm{N})\mathrm{NLO}})$.